Could SAFE concept be applied for designing a new synthetic aperture telescope?

Barak Katz* and Joseph Rosen

Department of Electrical and Computer Engineering,
Ben Gurion University of the Negev, P.O Box 653, Beer-Sheva 84105, Israel
**barakk@ee.bgu.ac.il*

Abstract: Synthetic aperture with Fresnel elements (SAFE) is an incoherent holographic imaging system in which the complete hologram is a mosaic of several holograms captured from different points of view. In this paper we investigate a new scheme of SAFE which may be used as a basis for designing a new type of synthetic aperture telescopes. Laboratory in-door experiments may provide the proof of concept for such a new design.

OCIS codes: (090.0090) Holography; (280.6730) Synthetic aperture radar; (110.6770) Telescopes; (050.1965) Diffractive lenses; (050.5080) Phase shift; (090.1760) Computer holography; (090.2890) Holographic optical elements; (110.3175) Interferometric imaging.

References and links

1. A. A. Michelson, "On the application of interference methods to astronomical measurements," Astrophys. J. **51**, 257–262 (1920).
2. P. R. Lawson, *Selected Papers on Long Baseline Stellar Interferometry*, (SPIE Press Book, 1997).
3. R. Okayasu, M. Inoue, N. Kawaguchi, S. Kameno, K. Shibata, and Y. Asaki, "Space VLBI satellite HALCA and its engineering accomplishments," Acta Astronaut. **50**(5), 301–309 (2002).
4. M. E. Testorf and M. A. Fiddy, "Superresolution imaging-revisited," Adv. Imaging Electron Phys. **163**, 165–218 (2010).
5. S. M. Beck, J. R. Buck, W. F. Buell, R. P. Dickinson, D. A. Kozlowski, N. J. Marechal, and T. J. Wright, "Synthetic-aperture imaging laser radar: laboratory demonstration and signal processing," Appl. Opt. **44**(35), 7621–7629 (2005).
6. V. Mico, Z. Zalevsky, P. García-Martínez, and J. García, "Synthetic aperture superresolution with multiple off-axis holograms," J. Opt. Soc. Am. A **23**(12), 3162–3170 (2006).
7. L. Martínez-León and B. Javidi, "Synthetic aperture single-exposure on-axis digital holography," Opt. Express **16**(1), 161–169 (2008).
8. G. Indebetouw, Y. Tada, J. Rosen, and G. Brooker, "Scanning holographic microscopy with resolution exceeding the Rayleigh limit of the objective by superposition of off-axis holograms," Appl. Opt. **46**(6), 993–1000 (2007).
9. B. Katz and J. Rosen, "Super-resolution in incoherent optical imaging using synthetic aperture with Fresnel elements," Opt. Express **18**(2), 962–972 (2010).
10. J. Rosen and G. Brooker, "Digital spatially incoherent Fresnel holography," Opt. Lett. **32**(8), 912–914 (2007).
11. J. Rosen and G. Brooker, "Fluorescence incoherent color holography," Opt. Express **15**(5), 2244–2250 (2007).
12. J. Rosen and G. Brooker, "Non-scanning motionless fluorescence three-dimensional holographic microscopy," Nat. Photonics **2**(3), 190–195 (2008).
13. B. Katz, D. Wulich, and J. Rosen, "Optimal noise suppression in Fresnel incoherent correlation holography (FINCH) configured for maximum imaging resolution," Appl. Opt. **49**(30), 5757–5763 (2010).
14. B. E. A. Saleh and M. C. Teich, *Fundamentals of Photonics*, 2nd ed. (Wiley, 2007) p. 7.
15. J. W. Goodman, *Introduction to Fourier Optics*, 2nd ed. (McGraw-Hill, 1996) pp. 66–73.

1. Introduction

Synthetic aperture is a well-known super-resolution methodology which elevates the imaging capabilities of various ground and satellite telescopes [1–3]. Synthetic aperture extends the resolution capabilities of an imaging system beyond the theoretical Rayleigh limit dictated by the system's real aperture [4]. Using this technique, several measurements acquired by an aperture-limited system, from various locations, are combined together into one large pattern which can be captured only by a virtual system equipped with a much wider synthetic aperture. Governed by this general principle, there are various types of synthetic aperture telescopes, such as the Michelson stellar interferometer [1] and the Very long baseline

#138862 - $15.00 USD Received 30 Nov 2010; revised 20 Feb 2011; accepted 21 Feb 2011; published 1 Mar 2011

interferometer (VLBI) [2,3]. Yet, these telescopes' image of objects, that are very far from the telescopes, is such that the curvature in the wavefronts arriving from the objects is negligible. Formally this condition is expressed by the inequality $z_s >> B^2/\lambda$, where B is the telescope baseline length, λ is the wavelength, and z_s is the distance from the telescope to the object.

The utilization of holographic imaging methods for synthetic aperture is usually restricted to coherent imaging [5–7]. Therefore, the use of this technique is limited only to those applications in which the observed targets can be illuminated by lasers. Synthetic aperture carried out by a combination of several off-axis incoherent holograms in scanning holographic microscopy has been demonstrated by Indebetouw *et al.* [8]. However, according to this method, although it is a technique of recording incoherent holograms, the object should also be illuminated by an interference pattern between two laser beams.

Synthetic aperture with Fresnel elements (SAFE) [9] represents a new type of passive incoherent holographic systems operating in a synthetic aperture mode. SAFE is passive in the sense that it images self illuminated objects or objects which are illuminated by other incoherent sources not related to SAFE. The term incoherent light here means quasi-monochromatic spatially incoherent light. The holographic concept is based on the recently invented Fresnel incoherent correlation hologram, dubbed FINCH [10–13]. In FINCH, incoherent light is reflected or emitted from a three dimensional object, then propagates through a spatial light modulator (SLM), and finally is recorded by a digital camera. The SLM's pattern is used as a diffractive beam splitter of the incoherent interferometer, so that each spherical beam, originated from each object point, is split into two spherical beams with two different curve radii. Accumulation of the entire interferences of all of the couples of spherical beams creates the Fresnel hologram of the observed object. Three holograms are recorded sequentially, each for a different phase factor of the SLM. The three holograms are superposed in the computer, so that the result is a complex-valued Fresnel hologram that does not contain the twin image and the bias term. SAFE digitally arranges several sub-holograms into a complete Fresnel hologram of the observed object, where each hologram is acquired by a limited-aperture FINCH-like system from different points of view. SAFE indeed improves the resolution performance of lensless FINCH, however the resolution gain in the earlier experiment has been less than the ratio between the synthetic and the real apertures [9].

In this paper we propose a new scheme of SAFE and investigate its potential in the future to become a telescope for imaging nearby objects. In contrast to the telescopes mentioned above, the distance to the objects of the proposed telescope is limited by the inequality $\boldsymbol{z_s} < B^2/\lambda$. Due to its potential task, and in order to distinguish it from earlier systems, we dub the present configuration 'telescopic SAFE' (T-SAFE). The term synthetic aperture herein means time (or space) multiplexing of several Fresnel holographic elements captured from various viewpoints by a system with a limited real aperture. The synthetic aperture is implemented by shifting the system, located across the field of view, among several viewpoints. At each viewpoint a different mask is displayed on the SLM, and a single element of the Fresnel hologram is recorded (See Fig. 1). The various holograms, each of which is recorded by the real aperture system during the capturing time, are tiled together so that the final mosaic hologram is effectively considered as captured from a single synthetic aperture which is much wider than the real aperture.

In T-SAFE, due to a modification of the original SAFE setup, the resolution gain is indeed equal to the ratio between the synthetic and real apertures. The lensless T-SAFE system contains a band-pass chromatic filter (BPF) if the source is polychromatic rather than quasi-monochromatic. In case T-SAFE is implemented using polarization-sensitive SLM, a polarizer is introduced to the system. However in the following we propose an alternative configuration of T-SAFE, and for such systems neither SLMs nor polarizers are needed. As in SAFE, the sub-holograms are recorded by a digital camera, then they are arranged in the computer, and the mosaic hologram is digitally reconstructed.

#138862 - $15.00 USD Received 30 Nov 2010; revised 20 Feb 2011; accepted 21 Feb 2011; published 1 Mar 2011

2. Analysis of telescopic SAFE

An example of the earlier SAFE system with the synthetic aperture, which is three times wider than the real aperture, can be seen in Fig. 1. To simplify the demonstration, the synthetic aperture was implemented only along the horizontal axis. In principle this concept can be generalized for both axes. In SAFE shown in Fig. 1, the whole system moves in front of the object. The complete Fresnel hologram of the object, located at some distance from the SLM, is a mosaic of 3 holographic elements, each of which is recorded from a different point of view by the system with the real aperture which is $A_x \times A_y$ in size. In this specific example, the complete hologram arranged from 3 holographic Fresnel elements has the synthetic aperture which is $3 \cdot A_x \times A_y$ in size, and it is 3 times larger than the real aperture at the horizontal axis. An object point located at point (x_s, y_s, z_s), at a distance z_s from the SLM, induces a tilted diverging spherical wave in the form of $C_1(x_s, y_s)Q[1/z_s]L[-x_s/z_s, -y_s/z_s]$ on SLM plane (x, y), where for the sake of simplification, the quadratic phase function is designated by function *Q*, which is expressed as $Q[s] = \exp\left[i\pi s\lambda^{-1}\left(x^2 + y^2\right)\right]$, and the linear phase function is designated by the function *L*, which is expressed as $L[s_x, s_y] = \exp\left[i2\pi\lambda^{-1}\left(s_x x + s_y y\right)\right]$. λ is the average wavelength and $C_1(x_s, y_s)$ is a complex constant dependent on the source point location.

Each tilted diverging spherical wave in the (m, n)-th exposure is split into two waves by the SLM mask. Based on our earlier experience with the technology of phase-only SLMs [9–13], the efficient way to split the wave is implemented by displaying one quadratic phase pattern on half of SLM pixels and one constant phase pattern on the other half of SLM pixels. This overall pattern is approximated by the following expression for the SLM *mn*-th sub-pattern $P_{mn}(x,y)$:

$$P_{mn}(x, y) = \left(C_2 Q[-1/f_d] + C_3\right) rect\left[\left(x - A_x \cdot m\right)/A_x, \left(y - A_y \cdot n\right)/A_y\right]. \qquad (1)$$

$P_{mn}(x,y)$ is a sum of aperture-limited quadratic phase and constant phase functions. f_d is a real constant indicating the focal distance of the diffractive lens, $C_{2,3}$ are complex constants, and

$$rect\left(\frac{x}{\alpha}, \frac{y}{\beta}\right) \equiv \begin{cases} 1 & \left(|x|, |y|\right) \le (\alpha/2, \beta/2) \\ 0 & \text{Otherwise.} \end{cases}$$

It should be noted that Eq. (1) is a mathematical simplification of the real SLM pattern because the general complex function $P_{mn}(x,y)$ is implemented by a phase-only SLM. Due to this simplification there is a gap between the predictions of the analysis and the experimental results. Fortunately, for T-SAFE as shown in the following, we have been capable of presenting an alternative method of displaying the two masks on the SLM, a method which is simple enough to be analyzed without any approximation. Therefore, the experimental results in this study are closer to the theoretical predictions than ever before [9–13]. However, before getting to the final configuration of T-SAFE, we analyze the prior SAFE from which T-SAFE

#138862 - $15.00 USD Received 30 Nov 2010; revised 20 Feb 2011; accepted 21 Feb 2011; published 1 Mar 2011

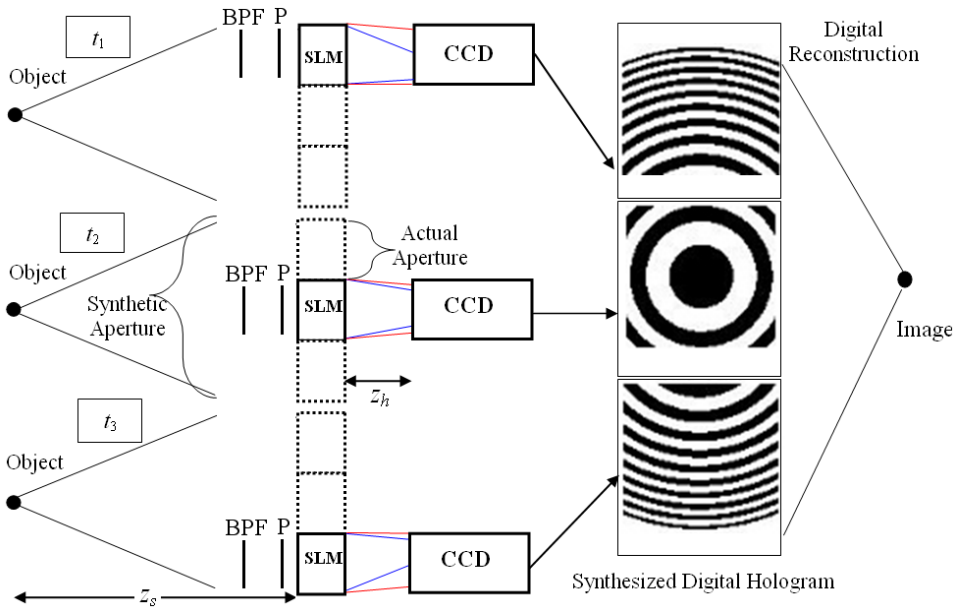

Fig. 1. Scheme of SAFE operating as synthetic aperture radar to achieve super-resolution. P, polarizer; BPF, bandpass filter; SLM, spatial light modulator; and CCD, charged coupled device.

has been unavoidably developed. Going back to the analysis of the system response to a point source, due to the SLM diffractive element we realize that there are two waves propagating from the SLM plane a distance z_h till they are recorded by the digital camera. The complex amplitude on the camera plane (x_o, y_o) is computed as a free-space propagation under Fresnel approximation or, in other words, as a convolution between the complex amplitude on the SLM and the function $Q[1/z_h]$. A complete Fresnel hologram of the object point located at (x_s, y_s, z_s) is a sum of $M \times N$ holographic elements, each of which is the intensity distribution recorded from the (m,n)-th location by the digital camera as the following:

$$I_h(x_o, y_o; x_s, y_s, z_s) = \sum_{n=\frac{1-N}{2}}^{\frac{N-1}{2}} \sum_{m=\frac{1-M}{2}}^{\frac{M-1}{2}} \left| C_1(x_s, y_s) Q\left[\frac{1}{z_s}\right] L\left[\frac{-x_s}{z_s}, \frac{-y_s}{z_s}\right] P_{mn}(x, y) * Q\left[\frac{1}{z_h}\right] \right|^2, \quad (2)$$

where the asterisk denotes a two dimensional convolution, and without the loss of generality, we assume that M and N are odd numbers. Neglecting diffraction effects of each aperture $A_x \times A_y$ along distance z_h and following straightforward calculations [9], the intensity distribution recorded by the digital camera is expressed by the following:

$$I_h(x_o, y_o; x_s, y_s, z_s) = \left(C_4 + C_5(x_s, y_s) Q\left[\frac{-1}{z_r}\right] L\left[\frac{x_r, y_r}{-z_r}\right] + C_5^*(x_s, y_s) Q\left[\frac{1}{z_r}\right] \times L\left[\frac{x_r, y_r}{z_r}\right] \right) \sum_{n=\frac{1-N}{2}}^{\frac{N-1}{2}} \sum_{m=\frac{1-M}{2}}^{\frac{M-1}{2}} rect\left(\frac{x_o - A_x \cdot m}{A_x}, \frac{y_o - A_y \cdot n}{A_y}\right), \quad (3)$$

where

#138862 - $15.00 USD Received 30 Nov 2010; revised 20 Feb 2011; accepted 21 Feb 2011; published 1 Mar 2011

$$z_r = \pm\frac{(z_s + z_h)(f_d z_s - z_h z_s + f_d z_h)}{z_s^2} \underset{z_s\to\infty}{\cong} \pm(f_d - z_h),$$

$$x_r = \frac{x_s z_h}{z_s}, \quad y_r = \frac{y_s z_h}{z_s},$$

and $C_{4,5}$ are complex constants. z_r is the reconstruction distance of the point image from an equivalent optical hologram, although in the present case the hologram is of course digital, and the reconstruction is done by the computer.

Equation (3) is the expression of the transparency function of a Fresnel hologram created by an object point and recorded by a conventional lensless FINCH [9] with a synthetic aperture which is $M \cdot A_x \times N \cdot A_y$ in size. The transverse magnification M_T is expressed as $M_T = \partial x_r / \partial x_s = z_h / z_s$. Assuming the FINCH system is diffraction limited, the minimum resolved object size is shown by:

$$\Delta_{\min} = \max\left\{\lambda / NA_{in}, \lambda / (M_T NA_{out})\right\} = \max\left\{2\lambda z_s / D_{SLM}, 2\lambda |z_r| / (M_T D_H)\right\}, \quad (4)$$

where D_{SLM}, D_H are the diameters of the SLM, and the digital hologram, respectively. NA_{in} and NA_{out} are the numerical aperture at the input and output of the complete holographic system, respectively. As expressed by Eq. (4), in FINCH the resolution limitation can be dictated by either input or output apertures. The NA_{in} is determined by the SLM size and cannot be changed by the system free parameters. However the product $NA_{out}M_T$ is dependent on the system parameters and our goal should be to keep this product equal or larger than NA_{in}, in order not to reduce the resolution dictated by the input aperture. Therefore, referring to Eq. (4), an optimal FINCH satisfies the inequality as follows:

$$\frac{z_s}{D_{SLM}} \geq \frac{|z_r|}{M_T D_H}. \quad (5)$$

In this inequality all the parameters are well defined except the diameter of the hologram. The hologram size is dependent on the overall size of the reconstructed image. Assuming the observed object is much smaller than the overall size of the field of view, as is frequently the case in telescopic observations, its image is much smaller than the SLM size. Figures 2(a) and 2(b) presents the two possible configurations of FINCH for the case of point-like image, one is for $f_d > z_h$ [2(a)] and the other is for $f_d < z_h$ [2(b)]. From Fig. 2 it is easy to see that the diameter of the hologram is determined by:

$$D_H = D_{SLM} \frac{|f_d - z_h|}{f_d}. \quad (6)$$

Substituting $M_T = z_h / z_s$, $|z_r| = |f_d - z_h|$ and Eq. (6) into Eq. (5) yield the following upper limit for the length of f_d:

$$f_d \leq z_h. \quad (7)$$

In other words the optimal configuration, in terms of resolution for T-SAFE, is achieved when the focal length of the positive diffractive lens displayed on the SLM is smaller than the distance between the SLM and CCD. This condition is fulfilled by the setup of Fig. 2(b). In this case, the resolution is determined by the input aperture and therefore, increasing synthetically the input aperture by N times improves the overall resolution by N times. It should be noted that, as has been demonstrated in Ref. [13], in case that the observed object

#138862 - $15.00 USD Received 30 Nov 2010; revised 20 Feb 2011; accepted 21 Feb 2011; published 1 Mar 2011

occupies most of the field of view, the image has the size of order of the SLM dimensions. In that case it can be assumed that $D_H \cong D_{SLM}$, and the system remains limited by the input aperture if $f_d \le 2z_h$. The lower limit of f_d for D_H in both abovementioned cases is determined by the SLM's pixel size Δ, and the number of pixels *K* along the SLM's diameter, according to the well-known inequality $f_d \ge K\Delta^2/\lambda$.

Under the condition of Eq. (7) it is obvious from Fig. 2(b) that if each sub-mask of T-SAFE contains both quadratic and constant phase pattern, the split waves are detected in two separated areas on the CCD and therefore there is no interference between them. In particular, in order to get interference between the spherical and the plane waves for every sub-hologram of T-SAFE and for every object point, we should use two separated sub-masks located at the two opposite sides of the optical axis, each one for different type of waves, the spherical and the plane waves. This situation is depicted in Fig. 2(c). We conclude that for the case of T-SAFE, contrary to SAFE, it is not enough to move the observation system as one unit, like it is shown in Fig. 1. In order to record each sub hologram, two optical elements have to be moved in two opposite directions as shown in Fig. 3. On the one hand this configuration has the disadvantage of shifting two elements in opposite directions, and of interfering the two waves from a distance that grows with the size of the synthetic aperture. In this sense T-SAFE

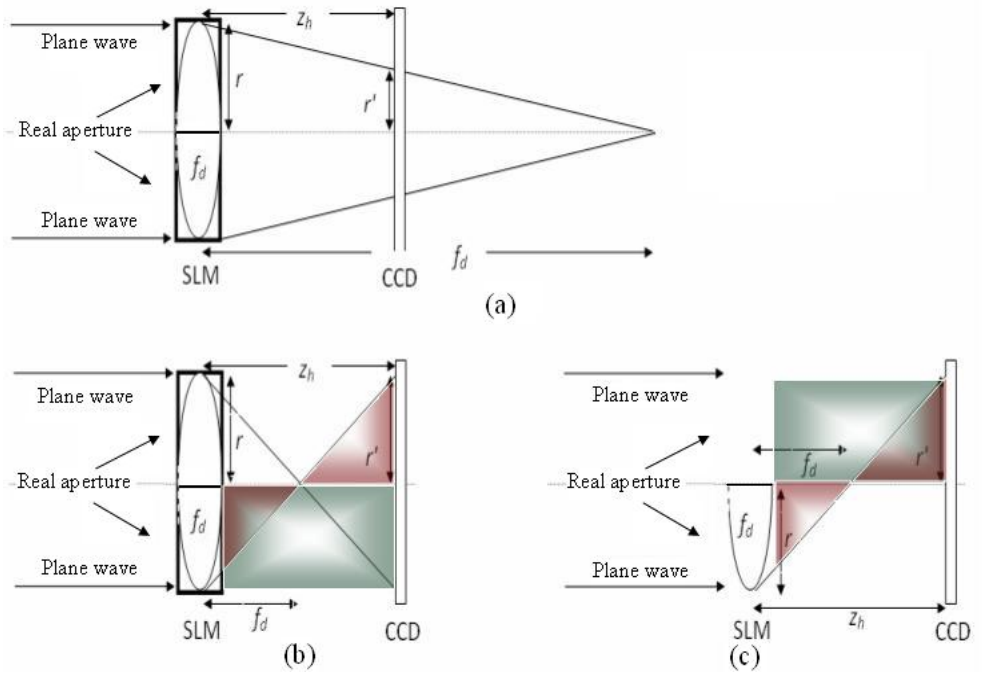

Fig. 2. Possible configurations of recording holograms in the case of point-like object: (a) for FINCH, where $f_d > z_h$. In this configuration a hologram can be recorded, but, as indicated in the text, this hologram is suboptimal. (b) for FINCH, where $f_d < z_h$. In this configuration a hologram cannot be recorded because there is no interference between the plane and the spherical waves arriving from the same part of the SLM. (c) for T-SAFE, where $f_d < z_h$. In this configuration the recorded hologram is optimal. The red and green areas indicate the spherical and plane waves, respectively. The rectangles in (a) and (b) symbolize the diffractive element of constant phase, where the lens symbol in all of the figures stands for the quadratic phase element, both the constant phase and quadratic phase elements are displayed on the same SLM.

is similar to the VLBI [2]. However, on the other hand, the important advantage of T-SAFE over SAFE and FINCH is that each phase function, the quadratic and the constant phases, are

#138862 - $15.00 USD Received 30 Nov 2010; revised 20 Feb 2011; accepted 21 Feb 2011; published 1 Mar 2011

displayed solely on a different optical element. Consequently we can display them directly on the phase-only SLM without any manipulations of spatial multiplexing. The analysis described above is no longer an approximation but an accurate description of the system. Moreover, since the most of large telescopes in the optical regime are equipped with mirrors, we suggest implementing T-SAFE with set of mirrors of two types, planar for the constant phase and spherical (or paraboloidal in case of non-paraxial imaging [14]) for the quadratic phase, as is shown in Fig. 3. Figure 3 presents four interfering steps needed to obtain the synthetic aperture hologram which is four times larger than the available real aperture. In this process, at each step, a different part of the complete quadratic function is carried out by the spherical mirror (or displayed on the SLM in our experiment). The converging spherical wave interferes with the wave arriving from the planar mirror located in the opposite side of the optical axis.

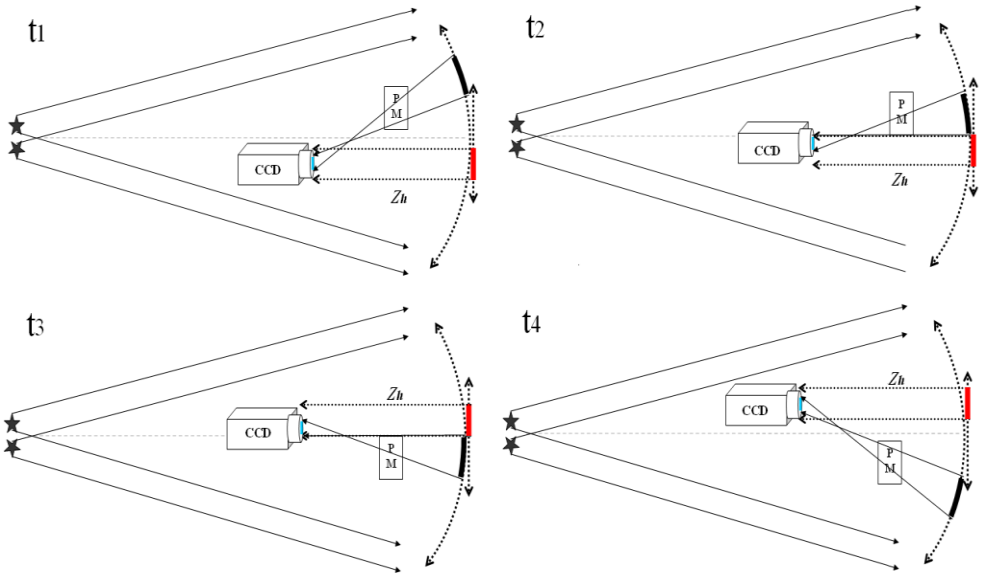

Fig. 3. Proposed design of T-SAFE which is based on spherical (black line) and flat (red line) mirrors rather than on SLMs. Four interfering steps, needed to obtain the synthetic aperture hologram, are shown. PM stands for phase modulator.

Note that in present in-door experiments the phase-only SLM is still used rather than the mirrors configuration, because it is easier to implement the phase shifting procedure by the SLM, and there is no need for an additional phase modulator as it is in case of the mirrors configuration.

The required *mn*-th sub-pattern $P_{mn}(x,y)$ for the *mn*-th sub-hologram of T-SAFE is given by the following expression:

$$P_{mn}(x,y) = C_2 Q\left[\frac{-1}{f_d}\right] rect\left[\frac{x - A_x(m+1/2)}{A_x}, \frac{y - A_y(n+1/2)}{A_y}\right] + C_3 rect\left[\frac{x + A'_x(m+1/2)}{A_x}, \frac{y + A'_y(n+1/2)}{A_y}\right]. \quad (8)$$

It is clear from Eq. (8) that the sub-pattern $P_{mn}(x,y)$ comprises two separate parts, one with the quadratic phase mask which is located at (mA_x,nA_y), and the other with the constant phase mask which is located at $(-mA'_x,-nA'_y)$, where the ratio between the steps of two parts is given by Eq. (9) as follows:

#138862 - $15.00 USD Received 30 Nov 2010; revised 20 Feb 2011; accepted 21 Feb 2011; published 1 Mar 2011

$$\frac{A_x'}{A_x}=\frac{A_y'}{A_y}=\frac{z_h-f_d}{f_d}. \tag{9}$$

The new point spread function (PSF) of the overall recording system of the entire $M \times N$ sub-hologram is given by Eqs. (2) and (3), where $P_{mn}(x,y)$ of Eq. (8) [instead of Eq. (1)] is substituted into Eq. (2), and the sums in Eqs. (2) and (3) count from (-{M,N}/2) to {M,N}/2-1, in which it is assumed this time that M and N are even numbers.

As mentioned earlier, Eq. (3) describes the Fresnel hologram obtained from a single object point, and therefore $I_h\left(x_o,y_o;x_s,y_s,z_s\right)$ is the PSF of the recording system in the synthetic aperture mode. The complete Fresnel hologram of a general incoherently-illuminated object $I_s\left(x_s,y_s,z_s\right)$ is an integral of the entire PSFs given by Eq. (3) over all object intensity distribution and is defined by Eq. (10) as follows:

$$H\left(x_o,y_o\right)=\iiint I_s\left(x_s,y_s,z_s\right)I_h\left(x_o,y_o;x_s,y_s,z_s\right)dx_s dy_s dz_s. \tag{10}$$

Since the overall PSF given in Eq. (3) is identical to the PSF of the previous works [10–13], the mosaic hologram given in Eq. (3) is a Fresnel incoherent hologram of the object but with the property that this hologram has been recorded with the effective aperture which is $M{\cdot}A_x \times N{\cdot}A_y$ in size.

The method to eliminate the twin image and the bias term [two terms out of three presented in Eq. (3)] is the same as has been used before [9–13]; three elemental holograms of the same object and for each point of view are recorded, where each of the SLM's phase mask has a different phase constant within the quadratic phase only. The final holographic element is a superposition of three recorded elements according to, for instance, Eq. (5) in Ref. [10]. The digital reconstruction of the final complex-valued mosaic hologram is conventionally computed by the Fresnel back propagation [15].

In the specific example where $I_s\left(x_s,y_s,z_s\right)$ contains two separated points, at $(x_{s1},y_{s1},-z_s)$ and $(x_{s2},y_{s2},-z_s)$, the complete Fresnel hologram, obtained from Eq. (3) after eliminating the twin image and the bias term, is as the following:

$$\begin{aligned} H\left(x_o,y_o\right)&=C_5\left(x_{s1},y_{s1}\right)Q\left[\frac{-1}{z_r}\right]L\left[\frac{\left(x_{r1},y_{r1}\right)}{-z_r}\right]+C_5\left(x_{s2},y_{s2}\right)Q\left[\frac{-1}{z_r}\right]L\left[\frac{\left(x_{r2},y_{r2}\right)}{-z_r}\right]\\ &=2C_5Q\left[\frac{-1}{z_r}\right]L\left[\frac{\left(x_{r1}+x_{r2}\right),\left(y_{r1}+y_{r2}\right)}{-2z_r}\right]\cos\left\{\frac{\pi}{\lambda z_r}\left[\left(x_{r2}-x_{r1}\right)x_o+\left(y_{r2}-y_{r1}\right)y_o\right]\right\}, \end{aligned} \tag{11}$$

where

$$x_{rk}=\frac{x_{sk}z_h}{z_s},\quad y_{rk}=\frac{y_{sk}z_h}{z_s},\quad k=1,2.$$

It is assumed in Eq. (11) that both object points are close enough to the origin so that we can assume $C_5\left(x_{s1},y_{s1}\right)\cong C_5\left(x_{s2},y_{s2}\right)=C_5$. According to Eq. (11), a feasible separation of two points at the object plane is subject to the ability to record at least one cycle of the cosine term by the effective aperture of the system.

3. Experimental results

T-SAFE has been tested in the lab by the system shown in Fig. 4. The tested object in all of the experiments has been represented by two uncorrelated point sources created by two independent HeNe lasers, each with 632 *nm* wavelength. The two laser beams have been focused by two lenses at focal distance of 6 *cm*, creating two diverging spherical waves with a transverse cross-section on the SLM plane that is much wider than the SLM size. One of the

#138862 - $15.00 USD Received 30 Nov 2010; revised 20 Feb 2011; accepted 21 Feb 2011; published 1 Mar 2011

lasers has been placed on top of a horizontal micrometer shifter to allow modification of the distances between the two point source objects. The distance z_s between the point source objects, i.e., from the back focal point of two lenses, and the SLM is 8 *m*. The distance z_h between the phase-only SLM (Holoeye, PLUTO, pixel size 8 μ*m*, 1080 × 1920 pixels array) and the digital camera (PixelFly, pixel size 6.7 μ*m*, 1024 × 1280 pixels array) is 88 *cm*. The real aperture in the experiments has been chosen to be one quarter of the complete physical aperture of the SLM, i.e., 1080 × 480 pixels, and the synthetic aperture has been chosen to be as large as the complete physical aperture of the SLM, i.e., 1080 × 1920 pixels.

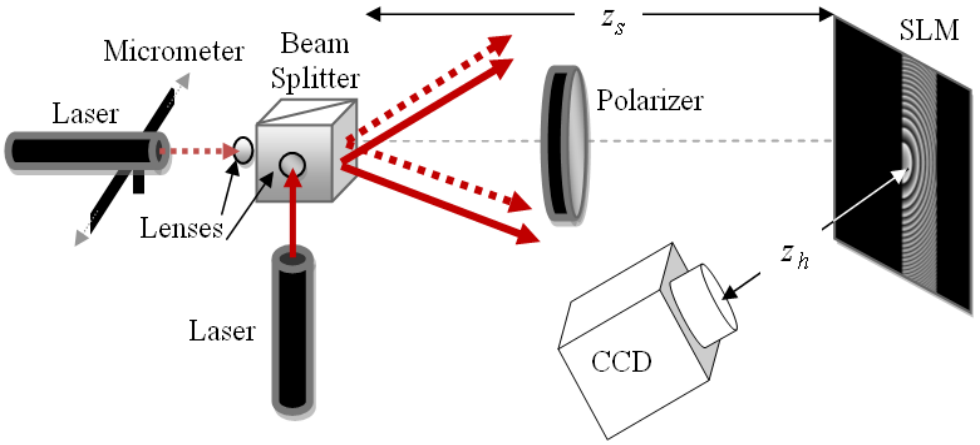

Fig. 4. Experimental setup. The two uncorrelated object points are created by two HeNe lasers and imaged by the T-SAFE.

The results of three conducted experiments are summarized in Fig. 5, Fig. 6, and Fig. 7, respectively. In the first experiment a comparison has been made between the complete aperture and the real aperture holograms recorded according to the setup of a regular FINCH. In the first experiment the gap between the points has been set at 1 *mm*. Figures 5(a)–5(d) show one of the three masks displayed on the SLM and their corresponding recorded [Fig. 5(b)] and computed [Fig. 5(c) magnitude and Fig. 5(d) phase] holograms for the complete aperture. Figures 5(e)–5(h) show the same, but this time the aperture is four times narrower. The focal distance of the diffractive lens on the SLM for both apertures is 55 *cm*. This focal distance guarantees optimal resolution, according to Eq. (7), and also assures that the complete hologram diameter obtained with the SLM full aperture is equal to the detector size, according to Eq. (6). Each of the three masks on the SLM has sequentially one of the three different phase factors: 0°, 120° or 240°. As mentioned above, these three phase masks with different phase constants are required in order to eliminate the bias term and the twin image from the holographic reconstruction.

The three recorded holograms are superposed according to the same superposition equation given in Ref. [10]. Figures 5(c), 5(d) and Figs. 5(g), 5(h) are the magnitude and the phase of the superposed holograms for the complete and the narrow apertures, respectively. Resolved and unresolved best in-focus reconstructed planes, for 1 *mm* gap between the source points, are shown in Fig. 5(i), for the complete, and in Fig. 5(j), for the narrow apertures, respectively. It can be seen that the resolution along the horizontal axis of the reconstructed image, computed by Fresnel back propagation, is worse for the narrow aperture than for the complete aperture because the hologram of the former contains less than one cycle of the cosine term presented in Eq. (11). In terms of the Raleigh criterion, our narrow aperture system can resolve a point gap larger than $1.22\lambda z_s / D$ = 1.6 *mm*, where z_s = 8 *m* and D = 480· 8 μm = 3840 μm is the width of the aperture. For comparison purposes, Fig. 5(k) and Fig. 5(l)

#138862 - $15.00 USD Received 30 Nov 2010; revised 20 Feb 2011; accepted 21 Feb 2011; published 1 Mar 2011

present the best in-focus reconstructed planes for a gap between the points that has been set to 1.5 *mm* and 2 *mm*, respectively. It can be seen that the narrow aperture system can hardly resolve a point gap of 1.5 *mm* as indicated by the Raleigh criterion, however for the 2 *mm* gap, a considerable separation is clearly seen.

In the second experiment, the synthetic aperture mechanism of T-SAFE has been tested and verified. In this occasion the distance z_h between the SLM and CCD and the focal distance of the diffractive lens displayed on the SLM have remained the same, 88 *cm* and 55 *cm*, respectively. Twelve different phase masks have been displayed on the SLM, three for each sub-aperture; left most, left, right and right most. Each of the masks has real aperture of 1080 × 480 pixels. In each of the four locations, masks at every location sequentially have one of the three different phase factors: 0°, 120° or 240°. The parts of the SLM, on which there is no quadratic function, use flat mirrors with the same constant phase value for the entire holograms.

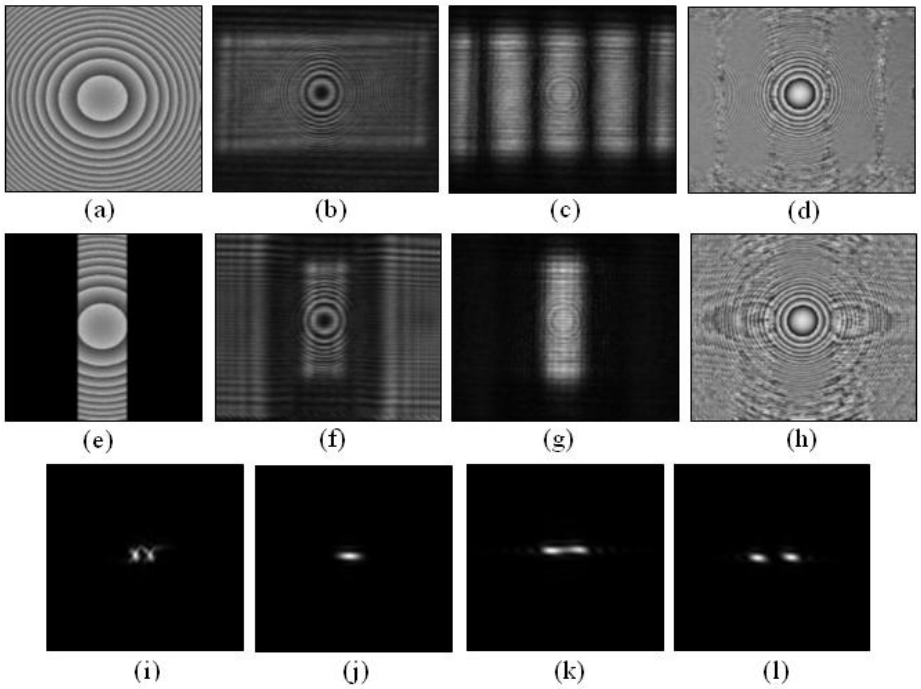

Fig. 5. Experimental results of a regular FINCH obtained for the complete and narrow apertures: (a) is one of the three masks displayed on the SLM for the complete wide aperture; (b) the corresponding recorded hologram; (c) the computed absolute and (d) phase of the complex-valued hologram of 1 *mm* gap between the source points; (e)-(h) the same as (a)-(d) but for the narrow aperture; (i) the best in-focus reconstructed plane in case of the complete aperture, for a gap between the source points of 1 *mm*; (j)-(l) the same as (i) but in case of narrow apertures for a gap between the source points of 1 *mm*, 1.5 *mm* and 2 *mm*, respectively.

Figures 6(a)–6(d) show the phase distribution of the four masks out of twelve, each of which has been displayed at different time and different location along the horizontal axis of the SLM. Note that unlike the masks of Fig. 5(a) and 5(e), in this T-SAFE experiment the masks of Figs. 6(a)–6(d) are purely quadratic phase on each of the four areas. Figures 6(e)–6(h) show the recorded holograms obtained after displaying the masks of Figs. 6(a)–6(d) on the SLM, respectively. The object in this experiment is again 2 source points separated by 1 *mm* gap. The superposed complex-valued holographic element from each system's viewpoint is stored in the computer. Upon completing the scanning procedure along the entire synthetic aperture, all four holographic elements are arranged as a single mosaic hologram. Figures 6(i)–6(l) and Figs. 6(m)–6(p) are, respectively, the magnitude and the phase of the

#138862 - $15.00 USD Received 30 Nov 2010; revised 20 Feb 2011; accepted 21 Feb 2011; published 1 Mar 2011

sub-holograms from which the synthetic aperture mosaic hologram is assembled. Figure 6(q) and Fig. 6(r) are the magnitude and the phase of the mosaic hologram, respectively. The best in-focus reconstruction result of the mosaic hologram, computed by the Fresnel back propagation, is depicted in Fig. 6(s). The two observed point source objects with a 1 *mm* gap between them are seen well in the reconstructed image, indicating that the synthetic aperture is wide enough to acquire the significant part of the horizontal spectral information of the objects.

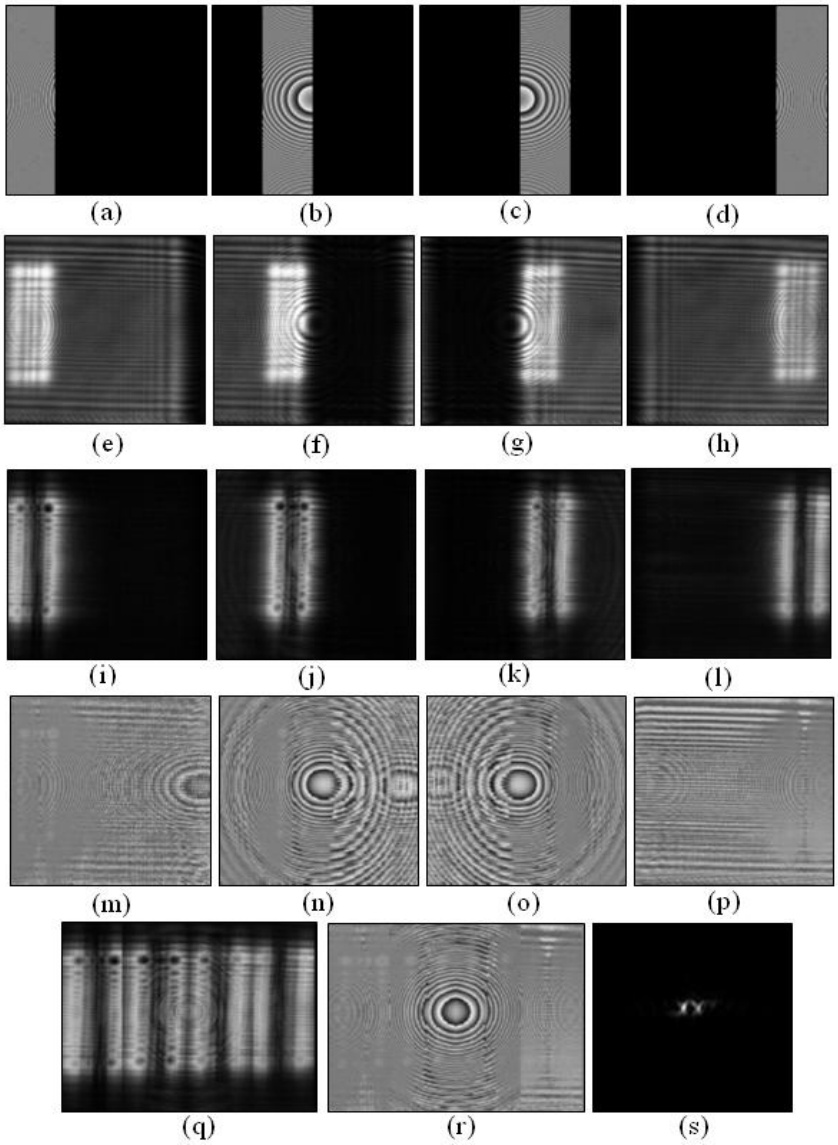

Fig. 6. Experimental results obtained for the case of synthetic aperture: (a)-(d) present four out of twelve masks displayed on the SLM during the recording process of the synthetic aperture hologram, and their corresponding recorded holograms are shown in (e-h); (i)-(l) computed magnitude and (m)-(p) phase of the complex holograms; (q) magnitude and (r) phase of the computed synthetic aperture hologram; (s) best in-focus reconstructed plane for the synthetic aperture for the gap between the points of 1 *mm*.

In the third experiment the synthetic aperture of T-SAFE has been tested for several different distances between the two point sources: 2 *mm* [Figs. 7(a)–7(c)], 1.5 *mm* [Figs. 7(d)–

#138862 - $15.00 USD Received 30 Nov 2010; revised 20 Feb 2011; accepted 21 Feb 2011; published 1 Mar 2011

7(f)], 1 mm [Figs. 7(g)–7(i)], and 0.75 *mm* [Figs. 7(j)–7(l)]. In Fig. 7, the hologram magnitudes are shown in the most left column, the phases are shown in the middle and best in-focus reconstructed planes of the synthetic aperture mosaic hologram are shown in the most right column.

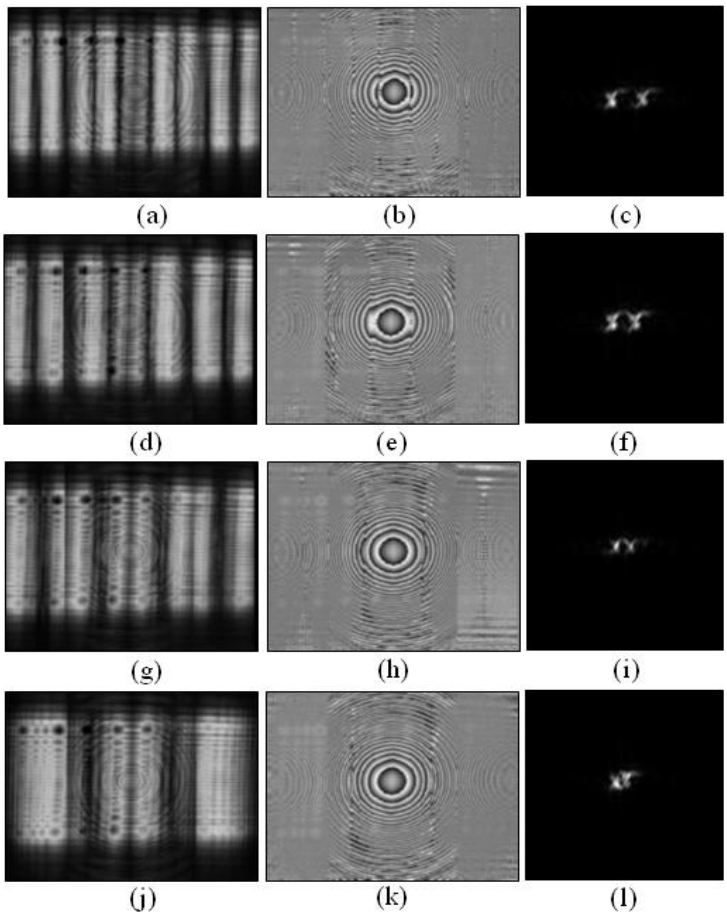

Fig. 7. Experimental results obtained for the case of synthetic aperture for several different distances between the two point objects: (a)-(c), (d)-(f), (g)-(i) and (j)-(l), show the magnitude, phase and best in-focus reconstructed planes for gaps between the points - 2 *mm*, 1.5 *mm*, 1 *mm and* 0.75 *mm*, respectively.

4. Discussion and conclusion

The main feature of T-SAFE is that its synthetic aperture increases the transverse resolving power by the ratio between the real and synthetic apertures. The captured hologram is of Fresnel rather than Fourier type, which means that the information distribution over the hologram can be controlled by modifying the system parameters. Drawing nearer to the image plane, by choosing f_d closer to z_h, also increases the similarity between the hologram and the observed object, whereas recording the hologram far from the image plane ($f_d << z_h$) distributes the recorded information more globally over the hologram plane. The nature of the observed objects determines which of the above options is preferred, but using Fresnel type holographic system enables us to choose between local and global distribution of the information.

Unlike the VLBI concept [2], T-SAFE does not sample the captured images, or to be more precise, it does not sample up to the level of the electrical detection. The mosaic hologram obtained by T-SAFE is equivalent to a single continuous Fresnel hologram captured once, by

#138862 - $15.00 USD Received 30 Nov 2010; revised 20 Feb 2011; accepted 21 Feb 2011; published 1 Mar 2011

a virtual system equipped with the wide synthetic aperture. In comparison to a hologram composed from spatial samples like in the VLBI, the hologram of T-SAFE contains more information which is actually the information of the samples and also information of adjacent areas. Even if the sub-holograms of T-SAFE are not spatially connected (scenario that has not been checked yet), the structure of the synthetic mosaic hologram consists of several non-connected patches and also contains more information than a hologram composed only from samples in the centers of these patches, that was the case with the VLBI.

Thus, in this study we have proposed and demonstrated a process of recording incoherent holograms in a synthetic aperture mode which may be used as a conceptual basis for a new type of incoherent synthetic aperture telescopes for relatively nearby objects.

Acknowledgements

We thank Gary Brooker of Johns Hopkins University for many fruitful discussions during the course of this project. We are also grateful to the anonymous reviewer for all his valuable comments and useful suggestions. This research was supported by Israel Ministry of Science and Technology (MOST) Grant GR-2234 (3-6807).

#138862 - $15.00 USD Received 30 Nov 2010; revised 20 Feb 2011; accepted 21 Feb 2011; published 1 Mar 2011